

Tunable wide-angle multi-band mid-infrared linear-to-linear polarization converter based on a graphene metasurface

Lan-Lan Zhang(张兰兰), Ping Li(李萍), and Xiao-Wei Song(宋霄薇)
Citation: Chin. Phys. B, 2021, 30 (**12**): 127803. DOI: 10.1088/1674-1056/ac0cdd
Journal homepage: http://cpb.iphy.ac.cn; http://iopscience.iop.org/cpb

What follows is a list of articles you may be interested in

Retrieval of the effective constitutive parameters from metamaterial absorbers

Shaomei Shi(石邵美), Xiaojing Qiao(乔小晶), Shuo Liu(刘朔), and Weinan Liu(刘卫南)
Chin. Phys. B, 2021, 30 (**11**): 117803. DOI: 10.1088/1674-1056/abff27

High-efficiency reflection phase tunable metasurface at near-infrared frequencies

Ce Li(李策), Wei Zhu(朱维), Shuo Du(杜硕), Junjie Li(李俊杰), and Changzhi Gu(顾长志)
Chin. Phys. B, 2021, 30 (**5**): 057802. DOI: 10.1088/1674-1056/abe9a6

Metamaterials and metasurfaces for designing metadevices: Perfect absorbers and microstrip patch antennas

Yahong Liu(刘亚红), Xiaopeng Zhao(赵晓鹏)
Chin. Phys. B, 2018, 27 (**11**): 117805. DOI: 10.1088/1674-1056/27/11/117805

Modeling for multi-resonant behavior of broadband metamaterial absorber with geometrical substrate

Kai-Lun Zhang(张凯伦), Zhi-Ling Hou(侯志灵), Song Bi(毕松), Hui-Min Fang(房惠敏)
Chin. Phys. B, 2017, 26 (**12**): 127802. DOI: 10.1088/1674-1056/26/12/127802

Metamaterials and plasmonics：From nanoparticles to nanoantenna arrays, metasurfaces, and metamaterials

Francesco Monticone, Andrea Alú
Chin. Phys. B, 2014, 23 (**4**): 047809. DOI: 10.1088/1674-1056/23/4/047809

Tunable wide-angle multi-band mid-infrared linear-to-linear polarization converter based on a graphene metasurface*

Lan-Lan Zhang(张兰兰)†, Ping Li(李萍), and Xiao-Wei Song(宋霄薇)

School of Medical Technology and Engineering, Henan University of Science and Technology, Luoyang 471000, *China*

(Received 14 April 2021; revised manuscript received 8 June 2021; accepted manuscript online 21 June 2021)

We present a high-efficiency tunable wide-angle multi-band reflective linear-to-linear (LTL) polarization converter, which is composed of an array of two L-shaped graphene patches with different sizes. In the mid-infrared region, the proposed converter can transform *x*-polarized wave into *y*-polarized wave at four resonant frequencies. The polarization conversion ratios of the four bands reach 94.4%, 92.7%, 99.3%, and 93.1%, respectively. By carefully choosing the geometric parameter, triple-band LTL polarization conversion can also be realized. The three polarization conversion ratios reach 91.50%, 99.20%, and 97.22%, respectively. The influence of incident angle on the performances of the LTL polarization converter is investigated, and it is found that our polarization converter shows the angle insensitivity. Also, the dynamically tunable properties of the proposed polarization converter are numerically studied by changing Fermi energy. All the simulation results are conducted by finite element method.

Keywords: metasurface, graphene, polarization converter, multi-band

PACS: 78.67.Wj, 61.48.Gh, 42.81.Gs **DOI:** 10.1088/1674-1056/ac0cdd

1. Introduction

Effectively manipulating the state of optical polarization is highly valuable.[1–3] Conventional polarization control methods usually include using optical grating, dichroic crystal, Faraday effects, and birefringent materials, *etc*.[4–6] These approaches require a long optical distance to accumulate the phase difference, which means that the traditional polarization devices are usually bulky and are not suitable for applications requiring miniaturization of optical elements. Therefore, it is urgent to develop new miniaturized polarization devices to meet many practical applications.

In recent years, metamaterials or metasurfaces have attracted increasing attention.[7,8] Researchers have found that they can easily modulate the polarization modes of electromagnetic (EM) waves.[9–13] To date, a series of novel polarization converters have been realized and studied by using metasurface,[14–20] which greatly promote the development of optoelectronics and optical communication. However, once these polarization converters are manufactured, most of them can neither be externally tuned nor electrically switched, which limits their development.

Graphene, a novel two-dimensional material, has aroused great interest of researchers in recent years. Graphene has high conductivity and can be continuously tuned by external electrostatic biasing,[21] which provides a bright perspective for the design of tunable optical devices.[22–26] Among these tunable devices, polarization converter is an indispensable component. Recently, many polarization converters have been reported by using graphene.[27–33] For example, Peng *et al.* reported a reflection-type polarization converter using graphene, which is composed of a strip-loaded half elliptical graphene ring array. The polarization converter not only convert linearly polarized incident wave into its cross-polarizations, but also convert circular polarization incident wave into its cross-polarizations.[34] Chen *et al.* proposed a tunable linear-to-linear (LTL) polarization converter by using hollowed "H" graphene patch array, which realized a broadband polarization conversion from 34.39 THz to 36.92 THz, and the polarization conversion ratio is more than 90%.[35] Peng *et al.* presented a tunable double-band LTL polarization converter in the THz region by using coupled graphene nanostructure. The polarization conversion phenomenon is achieved due to the hybridization effect caused by coupling interactions between plasmonic resonances in two graphene discs.[36] Zhu *et al.* proposed a broadband sinusoidally-slotted graphene-based cross-polarization converter structure, which realized a tunable broadband polarization conversion from 1.28 THz to 2.13 THz, and the polarization conversion ratio is more than 85%.[37] Zeng *et al.* proposed a dual-band cross-polarization converter by using U-shaped graphene nanostructures array.[38] Yao *et al.* proposed a triple-band LTL polarization converter based on graphene metasurface with double L-shaped unit. The polarization conversion ratios are 96.9%, 96.2%, and 83% at 36.15, 48.95, and 52.20 THz, respectively.[39] A triple-band cross-polarization conversion function was also realized by introducing slits into the elliptical graphene array. The polarization conversion ratio is more than 95% at the three operating frequencies.[40] The above

*Project supported by the School Youth Fund of Henan University of Science and Technology (Grant No. 2014QN045).

†Corresponding author. E-mail: zhanglan80515@163.com

© 2021 Chinese Physical Society and IOP Publishing Ltd

multi-band polarization converters are mostly double-band or triple-band. In practical applications, a four-band reflective LTL polarization converter is also needed. Recently, Chen *et al.* present a four-band reflective LTL polarization converter using two-layer graphene metasurface structure.[41] In their proposed polarization converter structure, two graphene metasurfaces are separated by the dielectric. Compared with the structure based on single-layer graphene, their fabrication is more difficult. To the best knowledge of the authors, four-band polarization converters based on single layer graphene metasurface have been rarely reported.

In this paper, a tunable wide-angle multi-band reflective LTL polarization converter using single-layer graphene metasurface is proposed and studied. It is a sandwich structure consisting of a single-layer graphene metasurface, a dielectric spacer, and a metal substrate. The single-layer graphene metasurface is composed of an array of two L-shaped graphene patches with different sizes. The polarization converter can transforms *x*-polarized wave into *y*-polarized wave at four resonance frequencies. A High-efficiency, three-band, LTL polarization conversion can also be realized by carefully selecting the geometric parameters. Furthermore, the polarization converter also presents good angular stability under oblique incidence angles, and the working frequency of the proposed polarization converter can be flexibly tuned by changing the Fermi energy without refabricating the structures. Our four-band polarization converter with simpler structure is easily fabricated, which has great application potential in electromagnetic polarization control.

2. Theoretical model and design

A generalized schematic of the proposed reflection wide-angle multi-band polarization converter is shown in Fig. 1(a). The structure consists of a graphene array at the top, a silica ($\varepsilon = 2.25$) dielectric spacer with thickness $t_s = 1000$ nm in the middle, and a metal gold substrate with thickness $t_m = 150$ nm at the bottom. Figure 1(b) shows one unit of the proposed structure. Here, graphene layer is composed of two L-shaped graphene sheets with different lengths and widths. d represents the distance between two L-shaped graphene, L_1 and W_1 represent the length and width of the larger L-shaped graphene patch, L_2 and W_2 represent the length and width of the smaller L-shaped graphene patch, P_x and P_y represents the periods in the x and y directions. The unit-cell has the following geometric parameters: $L_1 = 114$ nm, $W_1 = 62$ nm, $L_2 = 74$ nm, $W_2 = 37$ nm, $d = 6$ nm, $P_x = P_y = 160$ nm. The manufacturing processes of our proposed structure is feasible. In potential fabrication, the substrate gold layer can be obtained by electron beam evaporation, and the silica dielectric acts as an adhesive layer. A large-area graphene film can be fabricated by an optimized liquid precursor chemical vapor deposition method[42] and can be transferred onto silica layer. Two L-shaped array can be obtained by oxygen plasma etching and electron beam lithography.[43]

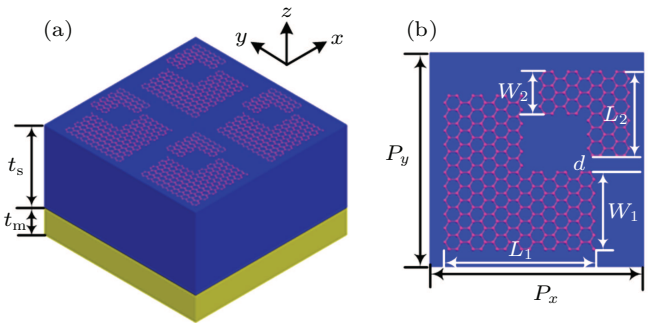


Fig. 1. (a) Schematic diagram of the proposed wide-angle multi-band polarization converter, where $t_m = 150$ nm, $t_s = 1000$ nm. (b) Unit cell of structure, where $L_1 = 114$ nm, $W_1 = 62$ nm, $L_2 = 74$ nm, $W_2 = 37$ nm, $d = 6$ nm, $P_x = P_y = 160$ nm.

The permittivity of metal gold substrate is described by the Drude model.[44] The graphene's relative permittivity ε_G can be obtained by[45]

$$\varepsilon_G = 1 + i\frac{\delta_G \eta_0}{(k_0 \Delta)}, \tag{1}$$

where, the impedance of air η is about 377 Ω, $\Delta = 1$ nm is the typical thickness of graphene thickness, δ_G represents the surface conductivity of graphene. In the mid-infrared range, δ_G can be calculated approximately as

$$\delta_G = \frac{ie^2 E_f}{\pi\hbar^2(\omega + i\tau^{-1})} + \frac{ie^2}{4\pi\hbar}\ln\left[\frac{2E_f - (\omega + i\tau^{-1})\hbar}{2E_f + (\omega + i\tau^{-1})\hbar}\right] + \frac{ie^2 k_B T}{\pi\hbar^2(\omega + i\tau^{-1})}\ln\left[\exp\left(-\frac{E_f}{k_B T}\right) + 1\right], \tag{2}$$

where, $\hbar$, k_B, and e represent the reduced Plank's constant, Boltzmann's constant, and electron charge, respectively. ω, T (= 300 K), τ and E_f are the angular frequency of the incident light, room temperature, electron scattering time, and Fermi energy level, respectively.

In our simulations, all the electromagnetic simulation results are obtained via the COMSOL software, which are based on the finite element method (FEM). A plane wave with an *x*-polarized electric field is used as the excitation source. The property of our proposed polarization converter can be described with a reflection matrix, which is as follows:[46]

$$R = \begin{pmatrix} R_{xx} & R_{xy} \\ R_{yx} & R_{yy} \end{pmatrix}, \tag{3}$$

where $R_{mn} = |E_m^r / E_n^i|$ (m, $n = x$, y), which represents the reflection coefficient, E_m^r represents the electric field of reflected wave with m polarization and E_n^i represents the electric field of incident wave with n polarization, the superscripts r and i are the abbreviations of the reflected and incident waves. In this paper, the incident wave is linearly *x*-polarized, and thus $R_{xy} = R_{yy} = 0$. Therefore, we only need to calculate R_{xx} and R_{yx} by assuming an *x*-polarized incidence.

To measure the polarization conversion performance, the polarization conversion ratio (PCR) is defined as[47,48]

$$\mathrm{PCR} = \frac{|R_{yx}|^2}{|R_{xx}|^2 + |R_{yx}|^2} \tag{4}$$

3. Results and discussion

The co-polarization reflection ($R_{xx} = |r_{xx}|^2$) and cross-polarization reflection ($R_{yx} = |r_{yx}|^2$) for normal incident are shown in Fig. 2(a), where $E_f = 1$ eV, $\tau = 1$ ps. It is clearly seen that there are four high reflection peaks in R_{yx} at 27.90, 33.35, 37.10, and 45.80 THz, respectively. On the contrary, four low reflection dips appear in R_{xx} at these four same frequencies. The PCR spectrum is shown in Fig. 2(b). The PCR spectrum shows four peaks which reach 94.4%, 92.7%, 99.3%, and 93.1% at 27.90, 33.35, 37.10, and 45.8 THz, respectively. These phenomena indicate that the designed structure can realize the four-band of polarization transfer from x to y direction. Figures 2(c)–2(f) depict the magnetic field profiles H_z on the surface of the graphene patch for 27.90, 33.35, 37.10, and 45.80 THz, respectively. The magnetic field distributions H_z are located on the edges of the graphene patch.

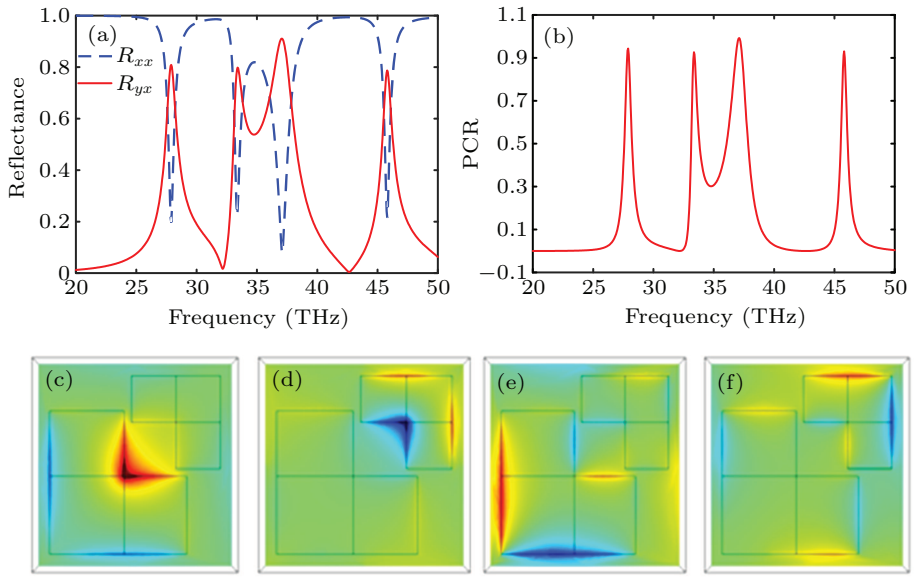


Fig. 2. Numerical results of the proposed wide-angle multi-band polarization polarization converter for normal incident. (a) Calculated co-polarization reflection (R_{xx}) and cross-polarization reflection (R_{yx}). (b) Calculated PCR spectrum; the magnetic field profiles H_z on the surface of the graphene patch for 27.90 THz (c), 33.35 THz (d), 37.10 THz (e), and 45.80 THz (f), respectively.

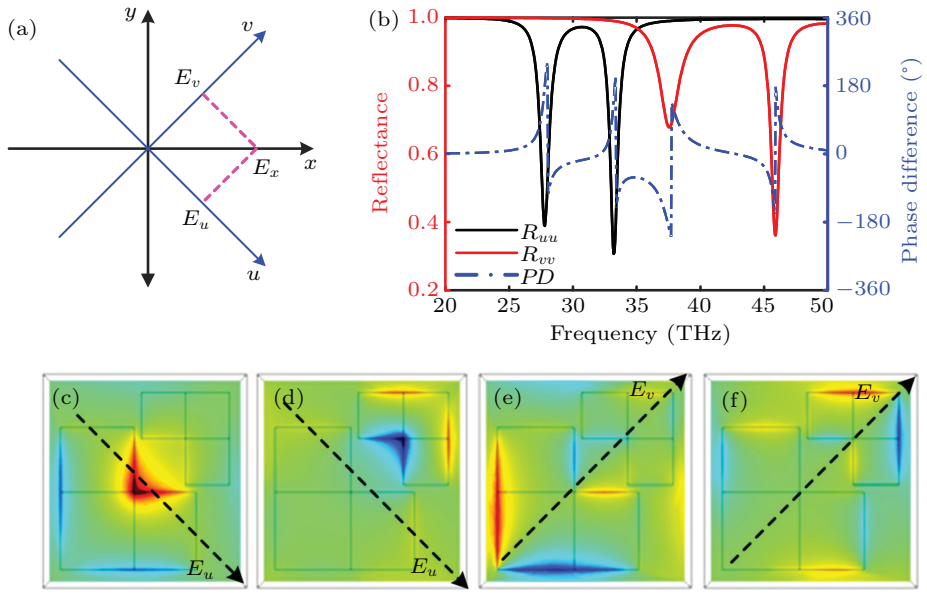


Fig. 3. (a) Schematic diagram of the decomposition of linearly polarized incident wave, (b) simulated co-polarization reflection (R_{uu}, R_{vv}) for polarization converter at incidences with $-45°$ (E_u) and $45°$ (E_v) polarizations. Panels (c)–(f) show the z component of the magnetic field distribution (H_z) at different frequencies (c) 27.90 THz with E_u incidence, (d) 33.50 THz with E_u incidence, (e) 37.10 THz with E_v incidence, and (f) 45.80 THz with E_v incidence, respectively.

To further reveal the physical mechanism of our proposed graphene-based polarization conversion, we analyzed the other two incident cases: E_u and E_v. For an x-polarized incident wave, it can be decomposed into two orthogonal polarized components with equal magnitudes and phases, here the u axis and the v axis are the directions that along 45° and −45° clockwise from the $+x$-axis direction, as shown in Fig. 3(a). Figure 3(b) shows two simulated reflection coefficients R_{uu} and R_{vv} under E_u and E_v incidences, respectively. There are two dips in R_{uu} at 27.90 THz, 33.35 THz and two dips in R_{vv} at 37.10 THz, 45.80 THz. These four dips originate from four eigenmodes, which are excited by E_u and E_v. The first two modes are excited by E_u polarization incidence at 27.90 THz and 33.35 THz, and the latter two modes are excited by E_v polarization incidence at 37.10 THz and 45.80 THz. These four modes are all derived from the excitation of the graphene surface plasmons (GSPs). The calculated PD $\Delta\varphi = \varphi_{vv}\varphi_{uu}$ is also shown in Fig. 3(b). $\Delta\varphi$ is close to 180°, 180°, −180°, and 0° at 27.90, 33.35, 37.10, and 45.8 THz. Therefore, at these four resonant frequencies, the superimposition of the two reflected components can produce the polarization rotation with rotation angle of 90°. The magnetic field profiles H_z at frequencies of 27.90 THz and 33.35 THz for E_u incidence are shown in Figs. 3(c) and 3(d), and these two eigenmodes show symmetric magnetic field distribution about the 45° direction. The magnetic field profiles H_z at frequencies of 37.10 THz and 45.80 THz for E_v incidence are shown in Figs. 3(e) and 3(f), and these two eigenmodes show anti-symmetrical magnetic field distribution about the 45° direction.

Figure 4 shows the simulated PCR under different incident angles, and the other parameters are the same with those of Fig. 2. The PCR is quite stable for the change of incident angle. When the incident angles increase from 0° to 60° four working frequencies of proposed polarization converter at 27.90, 33.35, 37.10, and 45.80 THz are almost unchanged, and the PCR peak values at these four resonant frequencies are also keep the same. Our polarization converter is based on four localized GSPs resonances, which are insensitive about the incident angle. The small feature size of graphene also contributes to the angle insensitivity of our device. In generally, at the same resonant frequency, the feature size of graphene plasmonic structure is several times smaller than the metal counterpart, which leads to less dependence on the incident angle.[30] When the incident angle is more than 60° the third PCR peak positions have obvious shift, and the PCR peak values of some resonant frequencies decrease. The reason is that the interaction between the electromagnetic wave and graphene is weakened under the large incident angle.[35] The simulation results imply that the proposed polarization converter is angle-insensitive.

To better understand the excitation of these plasmonic resonant modes, the geometric parameters L_1 and L_2 are changed for further study. The corresponding PCRs are illustrated in Figs. 5(a)–5(b), respectively. In Fig. 5(a), with the increase of L_1 (from 112 nm to 118 nm), we notice that the first and third PCR peak positions have obvious red-shifted, but the other two peak positions are almost unchanged, In Fig. 5(b), we notice that the second and fourth PCR peak positions have obvious red-shifted with the increase of L_2, while the position of other two peaks do not change significantly. When L_2 is reduced (from 74 nm to 68 nm), the third PCR peak and second PCR peak are close to each other. Finally, when $L_2 = 68$ nm, the second and third polarization conversion bands are coupled to each other, resulting in a wide polarization conversion band in which PCR is greater than 99.2% in the frequency range from 36.45 THz to 37.6 THz. Thus, a three-band polarization converter is achieved, and the three polarization conversion ratios reach 91.50%, 99.20%, and 97.22%, respectively. The above red-shift behavior shown in Figs. 5(a)–5(b) can be expected from the magnetic field profiles in Figs. 2(c)–2(f). It can be seen from Figs. 2(c) and 2(e) that the magnetic field energy is mainly distributed at the edges of the large L-shaped graphene patch for the frequencies of 27.90 THz and 37.10 THz. While the magnetic field energy is mainly distributed at the edges of the small L-shaped graphene patch for the frequencies of 33.35 and 45.80 THz, seen in Figs. 2(d) and 2(f). Therefore, the adjustment of geometric parameters of large L-shaped graphene patch (L_1) has a greater impact on the first and the third operating frequencies (27.90 THz and 37.10 THz) than the second and the fourth operating frequencies. But the second and the fourth operating frequencies (33.35 THz and 45.80 THz) are mainly dependent on geometric parameters of small L-shaped graphene patch (L_2).

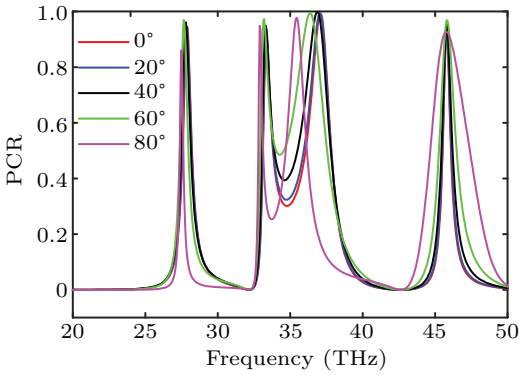


Fig. 4. Simulation of PCRs under different incident angles. Other parameters are the same as those in Fig. 2.

Next, the tunable properties of proposed four-band polarization conversion are discussed. It has been reported that the Femi energy of graphene can be tuned in the range of about −1 eV to 1eV by changing electrical gating,[49] which indicates that graphene has great potential in tunable devices. The PCRs for different graphene Fermi energy (E_f) are presented

in Fig. 6, other parameters are fixed as same as before. From Fig. 6, we can see that the PCRs are tunable over a wide range of frequencies. When E_f is decreased from 1 eV to 0.8 eV, four peaks of PCR are red-shifted from 27.90, 33.35, 37.10, and 45.80 THz to 25.00, 29.85, 33.25, and 40.90 THz, respectively. The reason of red-shift phenomenon is that the plasmonic resonant frequency (f) has a functional relationship with $(E_f)^{1/2}$.[50] Therefore, the decrease of E_f can result in the red-shift of the four peak positions.

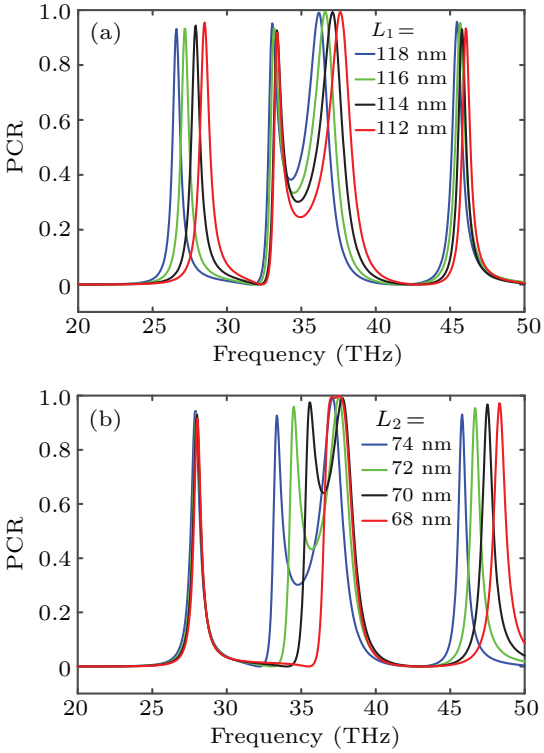


Fig. 5. Effects of geometric parameters on the performance of the proposed polarization converter. (a) Varying L_1, (b) varying L_2.

When $L_2 = 68$ nm, the PCRs of triple-band polarization conversion for different graphene Fermi energies (E_f) are presented in Fig. 7. The working frequencies of three-band polarization conversion are all red-shift with E_f decreasing from 1 eV to 0.8 eV. This phenomenon is attributed to the red shift of the GSPs' resonant frequency (f) with decreasing the Fermi energy (E_f).

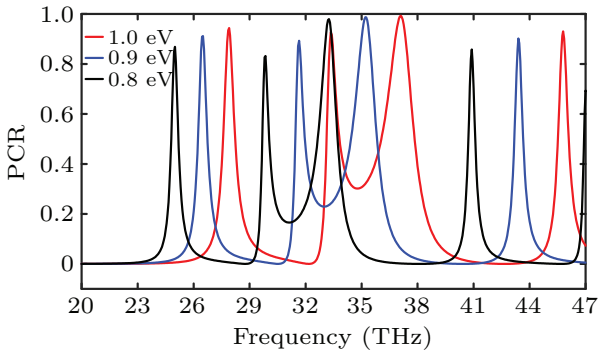


Fig. 6. Simulated PCRs of four-band LTL polarization converter for different graphene Fermi energies (E_f).

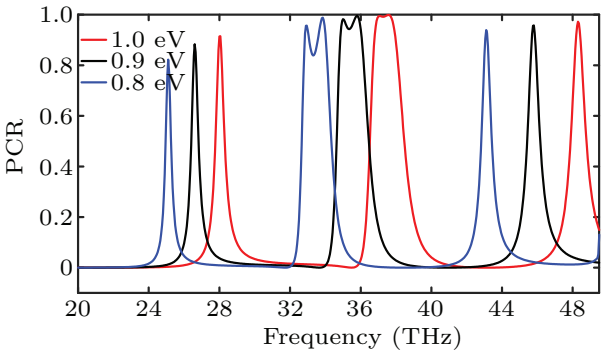


Fig. 7. Simulated PCRs of triple-band LTL polarization converter for different graphene Fermi energies (E_f).

Table 1. Comparisons of our proposed device with other graphene-based multi-band polarization converters.

References	Unit graphene shape	Single layer graphene or bilayer graphene	Band number	Working frequencies (THz)	PCR peaks (%)
[28]	L-shaped nanoslot	single layer graphene	two	31.45, 41.30	99, 97
[29]	ring embedded an ellipse resonator	single layer graphene	two	30.47, 33.14	96.74, 95.88
[32]	cross double-ellipse	single layer graphene	two	24.58, 26.43	97.22, 97.56
[36]	two discs	single layer graphene	two	47.0, 51.0	99.7, 99.5
[39]	double L-shaped	single layer graphene	three	36.15, 48.95, 52.20	96.9, 96.3, 83.0
[40]	ellipse patch with a slit	single layer graphene	three	28.70, 35.35, 39.00	98.29, 98.42, 97.64
[41]	twisting double L-shaped	bilayer graphene	four	21.30, 26.25, 28.65, 35.10	99.11, 99.47, 99.68, 99.60
This paper	two separated L-shapes with different sizes	single layer graphene	four	27.90, 33.35, 37.10, 45.80	94.4, 92.7, 99.3 93.1

We compared the key characteristics of our proposed device with other graphene based multi-band polarization converters reported in recent years. As shown in Table 1, the polarization converters based on single-layer graphene metasurface proposed in Refs. [28,29,32,36,39,40] are mostly double-band or triple-band. Although a four-band polarization converter is proposed in Ref. [41] it is based on bilayer grapehen metasurface. Compared with bilayer graphene-based polarization converter proposed in Ref. [41] our proposed single layer graphene-based structure has the characteristics of simpler structure and easier fabrication.

4. Conclusion

In summary, we proposed to achieve dynamically tunable multiple-band LTL polarization conversion by using a graphene metasurface, which is composed of an array of two L-shaped graphene patches with different sizes. The calculation results indicated that the proposed converter can transform *x*-polarized light into *y*-polarized light at four resonance frequencies simultaneously. The PCR can reach 94.4%, 92.7%, 99.3%, and 93.1% at 27.90, 33.35, 37.10, and 45.8 THz. Also, the dynamically tunable triple-band LTL polarization conversion can be realized by designing reasonable geometric parameters. The PCR can reach 91.50%, 99.20%, and 97.22%. The simulation results also indicate that the working frequency of the polarization converter can be easily tuned by changing the Fermi energy instead of redesigning the structure. Furthermore, our polarization converter shows good angle-independent property. We believe that our design will have potential applications in electromagnetic polarization control.

References

[1] Born M and Wolf E 1999 *Principles of Optics* (Cambridge: Cambridge University)
[2] Andreou A and Kalayjian Z 2002 *IEEE Sens. J.* **2** 566
[3] Ding S, Li R, Luo Y and Dang A 2018 *J. Opt. Soc. Am. A* **35** 1204
[4] Seshadri S 2001 *J. Opt. Soc. Am. A* **18** 1765
[5] Du G, Saito S and Takahashi M 2011 *Appl. Phys. Lett.* **99** 191107
[6] Zhang L, Zhong H, Deng C, Zhang C and Zhao Y 2010 *Opt. Express* **18** 20491
[7] Singh R, Plum E, Menzel C, Rockstuhl C, Azad A, Cheville R, Lederer E, Zhang W and Zheludev N 2009 *Phys. Rev. B.* **80** 153104
[8] Zhou L, Wang Y, Zhou J, Ding J, Su Z, Li M, Lu M, Shi H and Sang T 2020 *Appl. Phys. Express* **13** 042008
[9] Wu L, Yang Z, Cheng Y, Zhao M, Gong R, Zheng Y, Duan J and Yuan X 2013 *Appl. Phys. Lett.* **103** 021903
[10] Chin J, Lu M and Cui T 2008 *Appl. Phys. Lett.* **93** 251903
[11] Dong G, Shi H, Xia S, Li W, Zhang A, Xu Z and Wei X 2016 *Chin. Phys. B* **25** 084202
[12] Song K, Liu Y, Luo C and Zhao X 2014 *J. Phys. D: Appl. Phys.* **47** 505104
[13] Liu Y, Luo Y, Liu C, Song K and Zhao X 2017 *Appl. Phys. A* **123** 571
[14] Gao X, Han X, Cao W, Li H, Ma H and Cui T 2015 *IEEE Trans. Antennas Propag.* **63** 3522
[15] Li Y, Zhang J, Qu S, Wang J, Zheng L, Pang Y, Xu Z and Zhang A 2015 *J. Appl. Phys.* **117** 044501
[16] Ran Y, Shi L, Wang J, Wang S, Wang G and Liang J 2019 *Opt. Commun.* **451** 124
[17] Fahad A, Ruan C and Chen K 2019 *Electronics* **8** 869
[18] Pu Y, Luo Y, Liu L, He D, Xu H, Jiang H, Jiang Y and Liu Z 2018 *Chin. Phys. B* **27** 024202
[19] Zang X, Liu S, Gong H, Wang Y and Zhu Y 2018 *J. Opt. Soc. Am. B* **35** 950
[20] Chang C, Zhao Z, Li D, Taylor A, Fan S and Chen H 2019 *Phys. Rev. Lett.* **123** 237401
[21] Kovoselov K, Fal'ko V, Colombo L, Gellert P, Schwab M and Kim K 2012 *Nature* **490** 192
[22] Su Z, Wang Y, Luo X, Luo H, Zhang C, Li M, Sang T and Yang G 2018 *Phys. Chem. Chem. Phys.* **20** 14357
[23] Ye L, Sui K, Zhang Y and Liu Q 2019 *Nanoscale* **11** 3229
[24] Nikitin A, Guinea F, Garcia-Vidal F and Martin-Moreno L 2011 *Phys. Rev. B* **84** 161407
[25] Ye L, Chen Y, Cai G, Liu N, Zhu J, Song Z and Liu Q 2017 *Opt. Express* **25** 11223
[26] Mueller T, Xia F and Avouris P 2010 *Nat. Photon.* **4** 297
[27] Chen M, Sun W, Cai J, Chang L and Xiao X 2017 *Plasmonics* **12** 699
[28] Ding J, Arigong B, Ren H, Shao J, Zhou M, Lin Y and Zhang H 2015 *Plasmonics* **10** 351
[29] Guo T and Argyropoulos C 2016 *Opt. Lett.* **41** 5592
[30] Yang C, Luo Y, Guo J, Pu Y, He D, Jiang Y, Xu J and Liu Z 2016 *Opt. Express* **24** 16913
[31] Zhang L, Li P and Song X 2020 *J. Opt. Soc. Am. B* **37** 1921
[32] Yao Z, Wei T, Wang Y, Lu M, Zhang C and Zhang L 2019 *Appl. Opt.* **58** 3570
[33] Cheng H, Chen S, Yu P, Li J, Deng L and Tian J 2013 *Opt. Lett.* **38** 1567
[34] Peng L, Li X, Jiang X and Li S 2018 *J. Lightwave Technol.* **36** 4250
[35] Chen M, Chang L, Gao X, Chen H, Wang C, Xiao X and Zhao D 2017 *IEEE Photon. J.* **9** 4601011
[36] Peng J, Zhu Z, Zhang J, Yuan X and Qin S 2016 *Appl. Phys. Express* **9** 055102
[37] Zhu J, Li S, Deng L, Zhang C, Yang Y and Zhu H 2018 *Opt. Mater. Express* **8** 1164
[38] Zeng F, Ye L, Li L, Wang Z, Zhao W and Zhang Y 2019 *Opt. Express* **27** 33826
[39] Yao Z, Wang Y, Lu M and Zhang C 2019 *J. Opt. Soc. Am. B* **36** 7
[40] Zhang L, Li P and Song X 2020 *J. Opt. Soc. Am. B* **37** 1
[41] Chen M, Xiao X, Chang L, Wang C and Zhao D 2017 *Opt. Commun.* **394** 50
[42] Li X, Cai W, An J, Kim S, Nah J, Yang D, Piner R, Velamakanni A, Jung I, Tutuc E, Banerjee S, Colombo L and Ruoff R 2009 *Science* **324** 1312
[43] Abbas A, Liu G, Liu B, Zhang L, Liu H, Ohlberg D, Wu W and Zhou C 2014 *ACS Nano* **8** 1538
[44] Ordal M, Long L, Bell R, Bell S, Bell R, Alexander R and Ward C 1983 *Appl. Opt.* **22** 1099
[45] Yao Z, Wang Y, Lu M and Zhang C 2019 *J. Opt. Soc. Am. B* **36** 7
[46] Ding J, Arigong B, Ren H, Zhou M, Shao J, Lin Y and Zhang H 2014 *Opt. Express* **22** 29143
[47] Liu Z and Bai B 2017 *Opt. Express* **25** 8584
[48] Hao J, Ren Q, An Z, Huang X, Chen Z, Qiu M and Zhou L 2009 *Phys. Rev. A* **80** 023807
[49] Geim A 2009 *Science* **324** 1530
[50] Koppens F, Chang D and García de Abajo F 2011 *Nano Lett.* **11** 3370